ASME Journal of Mechanisms and Robotics
Online journal at:
https://asmedigitalcollection.asme.org/mechanismsrobotics

Sam O'Connor[1]
Department of Aerospace and Mechanical Engineering,
University of Notre Dame,
Notre Dame, IN 46556
e-mail: soconn22@nd.edu

Mark Plecnik[1,2]
Department of Aerospace and Mechanical Engineering,
University of Notre Dame,
Notre Dame, IN 46556
e-mail: plecnikmark@nd.edu

Aravind Baskar
Department of Aerospace and Mechanical Engineering,
University of Notre Dame,
Notre Dame, IN 46556
e-mail: abaskar@nd.edu

James Joo
Air Force Research Laboratory, Structures Technology Branch, Aerospace Systems Directorate,
Wright-Patterson Air Force Base,
OH 45433
e-mail: james.joo.1@us.af.mil

Complete Solutions for the Approximate Synthesis of Spherical Four-Bar Function Generators

Kinematic synthesis to meet an approximate motion specification naturally forms a constrained optimization problem. Instead of using local methods, we conduct global design searches by direct computation of all critical points. The idea is not new, but performed at scale is only possible through modern polynomial homotopy continuation solvers. Such a complete computation finds all minima, including the global, which allows for a full exploration of the design space, whereas local solvers can only find the minimum nearest to an initial guess. We form equality-constrained objective functions that pertain to the synthesis of spherical four-bar linkages for approximate function generation. We consider the general case where all mechanism dimensions may vary and a more specific case that enables the placement of ground pivots. The former optimization problem is shown to permit 268 sets of critical points, and the latter permits 61 sets. Critical points are classified as saddles or minima through a post-process eigenanalysis of the projected Hessian. The discretization points are contained within the coefficients of the stationarity polynomials, so the algebraic structure of the synthesis equations remains invariant to the number of points. The results of our computational work were used to design a mechanism that coordinates the folding wings. We also use this method to parameterize mechanism dimensions for a family of hyperbolic curves. [DOI: 10.1115/1.4064835]

Keywords: mechanism design, mechanism synthesis, mechanism synthesis and analysis

1 Introduction

The spherical four-bar is a single-degree-of-freedom mechanism with four links and four joints, whose axes all intersect at a single point in space. This mechanism is well-suited for the task of function generation, where the dimensions of the mechanism are synthesized to coordinate the rotation of the input link with the rotation of the output link in a desired manner. The synthesis of spherical four-bar function generators extends from the work of Freudenstein, where a number of desired mechanism configurations form a system of kinematic equations [1].

The kinematic synthesis for function generation involves the specification of input–output angles for the mechanism to pass through. To synthesize a spherical four-bar that can exactly reach these points in input–output space, a maximum of six angle pairs can be specified, as first noted by Roth [2]. Often in mechanical design, it is more beneficial to have a mechanism that approximates a specific function than one that meets a small number of points exactly. By specifying any number of angle pairs more than six for a spherical function generator to approximate, a designer can have more control over the function synthesized.

This paper provides a complete solution to the approximate synthesis of the spherical four-bars for two different cases: the most general case and with pre-specification of ground pivots (which is often practically sought). The complete solutions for common exact synthesis problems of spherical four-bar function generators are also reviewed. Our computational work is applied to the design of a mechanism which coordinates the timing of folding wings. Additionally, our work is used to parameterize the mechanism dimensions for a family of hyperbolic function specifications.

1.1 Literature Review.

The three-point function generation problem for the spherical four-bar was first solved by Hartenberg and Denavit [3]. The four, five, and six point exact synthesis problems were formulated by Zimmerman [4], Lakshminarayna [5], and Watanabe [6], respectively. More recent approaches to the five and six point problems have been shown with numerical results in Refs. [7,8]. The complete algebraic solution to the six-point problem was recently published by Jiawei et al. [9].

Approximate synthesis for the general case of spherical four-bar function generation was first considered by Rao and Ambekar [10]. In their approach, the interior penalty method was used to convert the constrained optimization problem to an unconstrained problem. An initial feasible point was found using the three-point

[1]Joint first authors.
[2]Corresponding author.

Contributed by the Mechanisms and Robotics Committee of ASME for publication in the Journal of Mechanisms and Robotics. Manuscript received November 1, 2023; final manuscript received February 8, 2024; published online May 23, 2024. Assoc. Editor: Dongming Gan.

exact synthesis method, and the Davidon–Fletcher–Powell method was used to iteratively solve a sequence of unconstrained optimization problems until the objective was below a certain threshold. In Liu and Angeles [11], the orthogonal decomposition algorithm, an iterative numerical method, was used to find a solution to the equality-constrained optimization. The formulation in Sancibrián et al. [12] uses the steepest descent to converge on local minima and requires a constraint equation for each prescribed position. In Alizade and Gezgin [13], the nonlinear equations from the stationarity conditions of the objective were converted to large square systems with nonlinear operators and solved numerically for a single solution. In a slightly different approach, Farhang and Zargar [14] applied perturbation theory to this approximate problem for the case where the input link is much smaller than the output link, and the motion of the output link is limited to small perturbations about some mean position. The approaches in Refs. [10–14] all rely on local optimization techniques, where an initial guess is used to find a single local minimum. Further, no previous literature has been found for the approximate synthesis case where the ground pivots are pre-specified.

In this paper, we formulate approximate kinematic synthesis as a constrained optimization problem. We next derive the classic Lagrangian stationarity conditions, but instead of using these conditions as a stopping criterion for an iterative search, we use them to directly compute all critical points of our optimization landscape. To elaborate, the stationarity conditions form a square polynomial system whose roots locate critical points. We apply the root-finding techniques of polynomial homotopy continuation to find all critical points of the optimization problem. It is true that within this complete set of critical points, one will always find the global minimum. However, Baskar et al. [15] have demonstrated a more compelling use for complete saddle point computations relevant to design optimization. Either way, our approach is tailored to enhance global *design exploration*, rather than *design tuning* which is more the realm of local optimizers that require starting guesses.

On a more detailed level, our formulation additionally collects all discretized task data into polynomial coefficients which multiply into our system through an organization of symmetric matrices. These matrices are formed from summations of specified task data, that may be numerically evaluated before root-finding begins. In this way, the computational cost of root finding remains independent from the number of task discretization points selected. This paper novelly formulates and summarizes the solution counts for (1) a spherical four-bar with both ground pivots pre-specified and (2) the general case with no pre-specifications. Both cases are *numerically reduced* following the methodology of parameter homotopy continuation [16]. The latter general case poses a greater computational challenge which was corralled by the method of random monodromy loops [17]. Despite posing a multihomogeneous degree of 621,984, the random monodromy loops algorithm took 5 min on a personal computer to find a maximum of 268 critical points for this optimization problem.

Our paper begins with a review of spherical four-bar kinematics (Sec. 2), and the solutions to the exact synthesis problems for five and six positions (Sec. 3–5). New complete solutions to the approximate synthesis problems are presented for the case when ground pivots are pre-specified (Sec. 6), and the general case when no dimensions are pre-specified (Sec. 7). Section 6 also highlights the collection of task data into polynomial coefficients to facilitate function evaluations for large numbers of discretization points. Section 8 details the application of our computational work to design a spherical four-bar for an aircraft application. The synthesis method is used to parameterize mechanisms with similar motions in Sec. 9. Conclusions are offered in Sec. 10.

2 Kinematics of a Spherical Four-Bar

A spherical four-bar is shown in Fig. 1. Its design is specified by the location of its four joint axes in a reference configuration, i.e.,

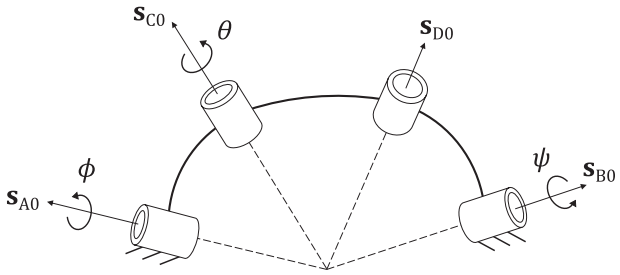

Fig. 1 Schematic of spherical four-bar

fixed joints $\mathbf{s}_{A0}$ and $\mathbf{s}_{B0}$, moving joints $\mathbf{s}_{C0}$ and $\mathbf{s}_{D0}$. Rotations about ground pivot $\mathbf{s}_{A0}$ are parameterized by ϕ. Rotations about ground pivot $\mathbf{s}_{B0}$ are parameterized by ψ. Rotation matrices written in axis-angle form are notated as $[\mathcal{R}(\mathbf{s}, \phi)]$. A rotation of $\mathbf{x}$ by ϕ about unit vector $\mathbf{s}$ evaluates to (Fig. 2)

$$[\mathcal{R}(\mathbf{s}, \phi)]\mathbf{x} = \mathbf{x} + \sin\phi\ \mathbf{s}\times\mathbf{x} + (1-\cos\phi)\ \mathbf{s}\times(\mathbf{s}\times\mathbf{x}) \tag{1}$$

A rotation of $\mathbf{s}_{C0}$ about $\mathbf{s}_{A0}$ yields the displaced vector

$$\mathbf{s}_C = [\mathcal{R}(\mathbf{s}_{A0}, \phi)]\mathbf{s}_{C0} \tag{2}$$

where the exclusion of zero from the subscript differentiates between the displaced and reference configurations of $\mathbf{s}_C$. Similarly, a rotation of $\mathbf{s}_{D0}$ about $\mathbf{s}_{B0}$ yields

$$\mathbf{s}_D = [\mathcal{R}(\mathbf{s}_{B0}, \psi)]\mathbf{s}_{D0} \tag{3}$$

The constraint of a spherical four-bar is that the relative angle between $\mathbf{s}_C$ and $\mathbf{s}_D$ remains constant throughout its motion. Therefore, the dot product of the vectors $\mathbf{s}_C$ and $\mathbf{s}_D$ should match the dot product of the vectors $\mathbf{s}_{C0}$ and $\mathbf{s}_{D0}$ at the reference configuration

$$\mathbf{s}_C \cdot \mathbf{s}_D = \mathbf{s}_{C0} \cdot \mathbf{s}_{D0} \tag{4}$$

Substituting Eqs. (2) and (3) in Eq. (4)

$$[\mathcal{R}(\mathbf{s}_{A0}, \phi)]\mathbf{s}_{C0} \cdot [\mathcal{R}(\mathbf{s}_{B0}, \psi)]\mathbf{s}_{D0} = \mathbf{s}_{C0} \cdot \mathbf{s}_{D0} \tag{5}$$

An explicit function of ψ in terms of ϕ can be found by first expanding (5) according to Eq. (1) to obtain

$$\mathcal{A}(\phi)\cos\psi + \mathcal{B}(\phi)\sin\psi + \mathcal{C}(\phi) = 0 \tag{6}$$

where

$$\mathcal{A}(\phi) = [\mathcal{R}(\mathbf{s}_{A0}, \phi)]\mathbf{s}_{C0} \cdot (\mathbf{s}_{D0} - (\mathbf{s}_{B0} \cdot \mathbf{s}_{D0})\mathbf{s}_{B0})$$
$$\mathcal{B}(\phi) = [\mathcal{R}(\mathbf{s}_{A0}, \phi)]\mathbf{s}_{C0} \cdot (\mathbf{s}_{B0} \times \mathbf{s}_{D0})$$
$$\mathcal{C}(\phi) = [\mathcal{R}(\mathbf{s}_{A0}, \phi)]\mathbf{s}_{C0} \cdot (\mathbf{s}_{B0} \cdot \mathbf{s}_{D0})\mathbf{s}_{B0} - \mathbf{s}_{C0} \cdot \mathbf{s}_{D0}$$

The well-known solution to Eq. (6) is provided by the explicit function

$$\psi = f(\phi) := \arctan\frac{\mathcal{B}(\phi)}{\mathcal{A}(\phi)} \pm \arccos\frac{-\mathcal{C}(\phi)}{\sqrt{\mathcal{A}(\phi)^2 + \mathcal{B}(\phi)^2}} \tag{7}$$

where either the "+" or "−" branch may be selected from the "±" symbol

3 Function Generation: General Setup

The goal of function generation is to synthesize a mechanism that coordinates the angle pairs (ϕ_j, ψ_j), $j = 0, 1, \ldots, N-1$. Without loss of generality to the function produced, one of the fixed axes should be specified. In the proceeding, we set $\mathbf{s}_{A0} = \{1, 0, 0\}$. A plane is spanned by $\mathbf{s}_{A0}$ and $\mathbf{s}_{B0}$. Without loss of generality to the function produced, any plane may be chosen. We choose to set both $\mathbf{s}_{A0}$ and $\mathbf{s}_{B0}$ into the $z = 0$ plane Therefore, in the proceeding, the second fixed axis takes the form $\mathbf{s}_{B0} = \{s_{Bx0},\ s_{By0},\ 0\}$.

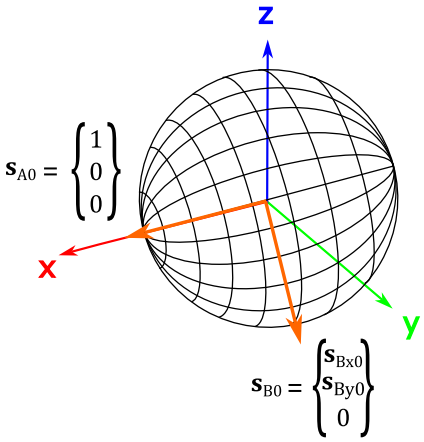

Fig. 2 General setup for spherical four-bar function generation

4 Exact Synthesis for Five Positions

Without loss of generality, any desired function may be shifted such that $(\phi_0, \psi_0) = (0, 0)$. The synthesis equations follow the form of Eq. (5)

$$[\mathcal{R}(\mathbf{s}_{A0}, \phi_j)]\mathbf{s}_{C0} \cdot [\mathcal{R}(\mathbf{s}_{B0}, \psi_j)]\mathbf{s}_{D0} = \mathbf{s}_{C0} \cdot \mathbf{s}_{D0}, \quad j = 1, \ldots, 4 \tag{8}$$

See that the index $j = 0$ is not used as it evaluates as identically true, reflective of the fact that $(\phi_0, \psi_0) = (0, 0)$ is automatically satisfied by virtue of choosing these angles to be measured from a reference configuration.

Following Sec. 3, the components of $\mathbf{s}_{B0}$, $\mathbf{s}_{C0}$, and $\mathbf{s}_{D0}$ serve as design variables ($\mathbf{s}_{A0}$ is set to $\{1, 0, 0\}$). For the case of five position synthesis, we elect to also set $\mathbf{s}_{B0}$, leaving the six components of $\mathbf{s}_{C0}$ and $\mathbf{s}_{D0}$ to form a simplified design space. These six variables must satisfy the four constraints of Eq. (8).

Note that $\mathbf{s}_{C0}$ and $\mathbf{s}_{D0}$ indicate directions, such that their magnitude is kinematically unimportant. Following this, one might set their magnitude to be unit by invoking two quadratic sphere constraints, $\mathbf{s}_{C0} \cdot \mathbf{s}_{C0} = 1$ and $\mathbf{s}_{D0} \cdot \mathbf{s}_{D0} = 1$. As an alternative, observe that the constraint of a constant dot product between $\mathbf{s}_C$ and $\mathbf{s}_D$ must adhere no matter their magnitudes. So instead of unity, we choose random magnitudes by invoking random linear cutting planes for $\mathbf{s}_{C0}$ and $\mathbf{s}_{D0}$

$$\mathbf{l}_C \cdot \mathbf{s}_{C0} = 1 \quad \text{and} \quad \mathbf{l}_D \cdot \mathbf{s}_{D0} = 1 \tag{9}$$

where $\mathbf{l}_C$ and $\mathbf{l}_D$ are random 3×1 vectors. These linear constraints are advantageous over sphere constraints due to their reduced degree.

Equations (8) and (9) are six equations in six unknowns: the components of $\mathbf{s}_{C0}$ and $\mathbf{s}_{D0}$. Over the complex numbers, these equations can be shown to generically have six finite, isolated solutions by choosing a multihomogeneous grouping that partitions the components of $\mathbf{s}_{C0}$ and $\mathbf{s}_{D0}$. The solutions to these equations can be obtained by many conventional means, and indicate spherical four bars that reproduce the desired function points, so long as branch or circuit defects are not present.

One of the six solutions is always a degenerate solution with no physical utility. This solution is the case where $\mathbf{s}_{C0}$ and $\mathbf{s}_{A0}$ are coincident and $\mathbf{s}_{D0}$ and $\mathbf{s}_{B0}$ are coincident. Since the moving joints are always aligned with the fixed joints, this solution can match any function, yet it has no practical value. However, since this solution is always real and complex solutions come in complex conjugate pairs, there will always be one real solution to this synthesis problem. Without considering the degenerate solution, this formulation admits five solutions, which is the same solution count shown algebraically in Ref. [5].

5 Exact Synthesis for Six Positions

In the formulation above, the components of $\mathbf{s}_{B0}$ were set rather than solved for. By leaving these components as unknowns, spherical four-bars can be computed that exactly reproduce the maximum number of six angle pairs. The constituent synthesis equations include Eq. (8), but now incremented from $j = 1, 2, 3, 4, 5$. Equation (9) is also reused. Similar to $\mathbf{s}_{C0}$ and $\mathbf{s}_{D0}$, the vector $\mathbf{s}_{B0}$ indicates an unknown direction. Dissimilar to $\mathbf{s}_{C0}$ and $\mathbf{s}_{D0}$, the vector $\mathbf{s}_{B0}$ must take unit magnitude, else Eq. (1) is no longer valid. Therefore, the quadratic circle constraint

$$\mathbf{s}_{B0} \cdot \mathbf{s}_{B0} = s_{Bx0}^2 + s_{By0}^2 = 1 \tag{10}$$

is appended to our synthesis equations. Note that Eq. (10) is a circle constraint and not a sphere constraint because, without loss of generality, s_{Bz0} is set to zero (Sec. 3). By modifying Eq. (8) to include $j = 5$, and combining it with Eqs. (9) and (10), a system of eight equations is formed in eight unknowns: two components of $\mathbf{s}_{B0}$, three components of $\mathbf{s}_{C0}$, and three components of $\mathbf{s}_{D0}$.

A three-homogeneous grouping partitioned by the vector components of $\mathbf{s}_{B0}$, $\mathbf{s}_{C0}$, and $\mathbf{s}_{D0}$, indicates a Bézout degree of 120. A more in-depth analysis computed by Bertini [18] found 14 finite, isolated solutions and 9 positive dimensional components. The isolated solutions occur in pairs that differ from each other by a 180° rotation about the x-axis. This is most readily identified by a sign flip of the variable s_{By0}. Since the members of each pair are easily obtained from one another, we only need to compute one member of each. Therefore, the number of isolated solutions to compute for the exact six position synthesis problem is only seven. This is the same solution count found algebraically in Ref. [9].

The positive dimensional components are split between a single quartic component of dimension 1, and eight linear components of dimension 2. The quartic component corresponds to the case when $\mathbf{s}_{C0}$ and $\mathbf{s}_{A0}$ are coincident, $\mathbf{s}_{D0}$ and $\mathbf{s}_{B0}$ are coincident, and $\mathbf{s}_{B0}$ may point in any direction of the x–y plane. The quartic algebraic variety is defined by

$$\mathbf{s}_{B0} \cdot \mathbf{s}_{B0} = 1, \quad (\mathbf{l}_C \cdot \mathbf{s}_{A0})\mathbf{s}_{C0} = \mathbf{s}_{A0}, \quad (\mathbf{l}_D \cdot \mathbf{s}_{B0})\mathbf{s}_{D0} = \mathbf{s}_{B0} \tag{11}$$

Two of the linear components correspond to the case when $\mathbf{s}_{A0}$, $\mathbf{s}_{B0}$, and $\mathbf{s}_{C0}$ are simultaneously coincident

$$\begin{aligned} s_{Bx0} &= \pm 1, & (\mathbf{l}_C \cdot \mathbf{s}_{A0})\mathbf{s}_{C0} &= \mathbf{s}_{A0}, \\ s_{By0} &= 0, & \mathbf{l}_D \cdot \mathbf{s}_{D0} &= 1 \end{aligned} \tag{12}$$

Another two correspond to the case when $\mathbf{s}_{A0}$, $\mathbf{s}_{B0}$, and $\mathbf{s}_{D0}$ are simultaneously coincident

$$\begin{aligned} s_{Bx0} &= \pm 1, & \mathbf{l}_C \cdot \mathbf{s}_{C0} &= 1, \\ s_{By0} &= 0, & (\mathbf{l}_D \cdot \mathbf{s}_{A0})\mathbf{s}_{D0} &= \mathbf{s}_{A0} \end{aligned} \tag{13}$$

The final four linear components take on complex values defined by certain special conditions. These can be summarized in the following two equations, denoting two components each

$$\begin{aligned} s_{Bx0} = \pm 1, \quad s_{By0} = 0, \quad & \mathbf{l}_C \cdot \mathbf{s}_{C0} = 1, \\ \frac{s_{Cy0}}{s_{Cz0}} = \frac{s_{Dy0}}{s_{Dz0}} = i, \quad & \mathbf{l}_D \cdot \mathbf{s}_{D0} = 1 \end{aligned} \tag{14}$$

$$\begin{aligned} s_{Bx0} = \pm 1, \quad s_{By0} = 0, \quad & \mathbf{l}_C \cdot \mathbf{s}_{C0} = 1, \\ \frac{s_{Cy0}}{s_{Cz0}} = \frac{s_{Dy0}}{s_{Dz0}} = -i, \quad & \mathbf{l}_D \cdot \mathbf{s}_{D0} = 1 \end{aligned} \tag{15}$$

Here i represents complex unit number.

6 Approximate Synthesis With Both Ground Pivots Specified

Now we alter the goal to only approximately reproduce the angle pairs, (ϕ_j, ψ_j), $j = 0, 1, \ldots, N-1$. For this formulation N must be greater than five. In this case, we must modify our constraint of a

constant dot product from Eq. (8)

$$\eta_j := [\mathcal{R}(\mathbf{s}_{A0}, \phi_j)]\mathbf{s}_{C0} \cdot [\mathcal{R}(\mathbf{s}_{B0}, \psi_j)]\mathbf{s}_{D0} - R_{CD} \quad j = 0, 1, \ldots, N-1 \tag{16}$$

Compared to Eq. (8), we have introduced a new variable R_{CD}, which is only approximately equal to $\mathbf{s}_{C0} \cdot \mathbf{s}_{D0}$. Despite this inexactness, we substituted in R_{CD}. Also, we included the $j = 0$ index, moved all variables to one side, and defined the resulting expression as η_j. For the approximate case, the angle pair $(\phi_0, \psi_0) = (0, 0)$ generally will not be exactly reproduced. Therefore, the dot product $\mathbf{s}_{C0} \cdot \mathbf{s}_{D0}$ will not hold constant at latter configurations, necessitating the introduction of the unknown dot product value R_{CD}. Following this vein, Eq. (16) will not evaluate to identically zero at the $j = 0$ configuration, hence its reinstatement compared to the exact case, Eq. (8).

If the jth angle pair were to be exactly met, then $\eta_j = 0$. The objective is then to minimize the sum of squares of η_j

$$f := \frac{1}{2}\sum_{j=0}^{N-1} \eta_j^2 \tag{17}$$

For brevity of notation, we omit summation indices in the proceeding because they generally do not change. Unless otherwise noted, assume $j = 0, 1, \ldots, N-1$. For this case, we are taking the values of both ground pivots $\mathbf{s}_{A0}$ and $\mathbf{s}_{B0}$ to be preset, leaving $\mathbf{s}_{C0}$, $\mathbf{s}_{D0}$, and R_{CD} as design variables to solve for.

The simplification invoked in Eq. (9) cannot be used for the approximate case. If $\mathbf{s}_{C0}$ and $\mathbf{s}_{D0}$ are not unit magnitude, it can be shown that the squared product of these magnitudes factor out of the summation of Eq. (17),

$$f := (|\mathbf{s}_{C0}||\mathbf{s}_{D0}|)^2 \left(\frac{1}{2}\sum \eta_j^2\right) \tag{18}$$

In this way, the objective can be interpreted as simultaneously minimizing the lengths of $\mathbf{s}_{C0}$ and $\mathbf{s}_{D0}$ according to each's intersection with a random cutting plane, as well as minimizing the intended objective. This unintentionally skews the landscape of the objective, therefore, constraints (9) are not invoked and instead quadratic sphere constraints are used

$$\mathbf{s}_{C0} \cdot \mathbf{s}_{C0} = 1 \quad \text{and} \quad \mathbf{s}_{D0} \cdot \mathbf{s}_{D0} = 1 \tag{19}$$

The following optimization problem has been framed:

$$\begin{aligned} \min_{\mathbf{s}_{C0}, \mathbf{s}_{D0}, R_{CD}} \quad & \frac{1}{2}\sum \eta_j^2 \\ \text{s.t. } \mathbf{h} := & \begin{Bmatrix} \mathbf{s}_{C0} \cdot \mathbf{s}_{C0} - 1 \\ \mathbf{s}_{D0} \cdot \mathbf{s}_{D0} - 1 \end{Bmatrix} = 0 \end{aligned} \tag{20}$$

The corresponding Lagrangian is

$$\mathcal{L} := \frac{1}{2}\sum \eta_j^2 + \mathbf{h}^T\boldsymbol{\lambda} \tag{21}$$

where $\boldsymbol{\lambda} = \{\lambda_1, \lambda_2\}$ are Lagrange multipliers. Before forming the stationarity conditions, introduce the following relative rotation matrices:

$$\begin{aligned} [\mathcal{R}_j] &= [\mathcal{R}(\mathbf{s}_{B0}, \psi_j)]^T[\mathcal{R}(\mathbf{s}_{A0}, \phi_j)], \quad j = 0, 1, \ldots, N-1 \\ &= \begin{bmatrix} \mathbf{c}_{xj} & \mathbf{c}_{yj} & \mathbf{c}_{zj} \end{bmatrix} = \begin{bmatrix} \mathbf{r}_{xj} \\ \mathbf{r}_{yj} \\ \mathbf{r}_{zj} \end{bmatrix} \end{aligned} \tag{22}$$

The columns of $[\mathcal{R}_j]$ are notated $\mathbf{c}_{xj}$, $\mathbf{c}_{yj}$, $\mathbf{c}_{zj}$, and its rows are $\mathbf{r}_{xj}$, $\mathbf{r}_{yj}$, $\mathbf{r}_{zj}$. The partial derivative of $\mathcal{L}$ may then be written

$$\frac{\partial \mathcal{L}}{\partial \mathbf{s}_{C0}} = \sum((\mathbf{s}_{C0} \cdot [\mathcal{R}_j]^T\mathbf{s}_{D0} - R_{CD})[\mathcal{R}_j]^T)\mathbf{s}_{D0} + 2\lambda_1\mathbf{s}_{C0} \tag{23}$$

$$\frac{\partial \mathcal{L}}{\partial \mathbf{s}_{D0}} = \sum(([\mathcal{R}_j]\mathbf{s}_{C0} \cdot \mathbf{s}_{D0} - R_{CD})[\mathcal{R}_j])\mathbf{s}_{C0} + 2\lambda_2\mathbf{s}_{D0} \tag{24}$$

$$\frac{\partial \mathcal{L}}{\partial R_{CD}} = -\sum([\mathcal{R}_j]\mathbf{s}_{C0} \cdot \mathbf{s}_{D0} - R_{CD}) \tag{25}$$

$$\frac{\partial \mathcal{L}}{\partial \boldsymbol{\lambda}} = \begin{Bmatrix} \mathbf{s}_{C0} \cdot \mathbf{s}_{C0} - 1 \\ \mathbf{s}_{D0} \cdot \mathbf{s}_{D0} - 1 \end{Bmatrix} \tag{26}$$

Equations (23)–(26) comprise of nine polynomials in nine variables: three components of $\mathbf{s}_{C0}$, three components of $\mathbf{s}_{D0}$, R_{CD}, λ_1, and λ_2. The roots of Eqs. (23)–(26) indicate the critical points of the optimization problem (20). Collecting coefficients rearranges the form of Eqs. (23)–(26) to make it more efficient for computations that involve a large number of discretization points.

To perform this collection, let's first consider Eq. (23). By expansion and application of the vector triple product identity, Eq. (23) may be rewritten

$$\begin{aligned} \frac{\partial \mathcal{L}}{\partial \mathbf{s}_{C0}} = \sum &([\mathcal{R}_j]^T\mathbf{s}_{D0} \times ([\mathcal{R}_j]^T\mathbf{s}_{D0} \times \mathbf{s}_{C0}) \\ &- [\mathcal{R}_j]^T\mathbf{s}_{D0}R_{CD} + (\mathbf{s}_{D0} \cdot \mathbf{s}_{D0})\mathbf{s}_{C0}) + 2\lambda_1\mathbf{s}_{C0} \end{aligned} \tag{27}$$

The collection of j indexed terms is straightforward except for the first term in the summation. To rearrange it into an amenable format, breakdown the following matrix multiplication:

$$[\mathcal{R}_j]^T\mathbf{s}_{D0} = \mathbf{r}_{xj}s_{Dx0} + \mathbf{r}_{yj}s_{Dy0} + \mathbf{r}_{zj}s_{Dz0} \tag{28}$$

where $\mathbf{r}_{xj}$, $\mathbf{r}_{yj}$, $\mathbf{r}_{zj}$ were introduced as the rows of $[\mathcal{R}_j]$ in Eq. (22). Then the first term of Eq. (27) may be rewritten

$$\begin{aligned} [\mathcal{R}_j]^T\mathbf{s}_{D0} \times ([\mathcal{R}_j]^T\mathbf{s}_{D0} \times \mathbf{s}_{C0}) &= (\mathbf{r}_{xj}s_{Dx0} + \mathbf{r}_{yj}s_{Dy0} + \mathbf{r}_{zj}s_{Dz0}) \\ &\quad \times (\mathbf{r}_{xj} \times \mathbf{s}_{C0}s_{Dx0} + \mathbf{r}_{yj} \times \mathbf{s}_{C0}s_{Dy0} \\ &\quad + \mathbf{r}_{zj} \times \mathbf{s}_{C0}s_{Dz0}) \\ &= \sum_{i=x,y,z}\sum_{k=x,y,z}(\mathbf{r}_{ij} \times (\mathbf{r}_{kj} \times \mathbf{s}_{C0})s_{Di0}s_{Dk0}) \end{aligned} \tag{29}$$

The cross products of Eq. (29) can be traded out for skew symmetric matrices. We notate skew symmetric matrices with the tilde "~" accent such that

$$\text{for } \mathbf{r} = \begin{Bmatrix} x \\ y \\ z \end{Bmatrix}, \quad \text{then } [\tilde{r}] := \begin{bmatrix} 0 & -z & y \\ z & 0 & -x \\ -y & x & 0 \end{bmatrix} \tag{30}$$

Then Eq. (29) can be rewritten

$$\begin{aligned} &[\mathcal{R}_j]^T\mathbf{s}_{D0} \times ([\mathcal{R}_j]^T\mathbf{s}_{D0} \times \mathbf{s}_{C0}) \\ &\quad = \sum_{i=x,y,z}\sum_{k=x,y,z}([\tilde{r}_{ij}][\tilde{r}_{kj}]\mathbf{s}_{C0}s_{Di0}s_{Dk0}) \end{aligned} \tag{31}$$

Expansion of the right-hand side yields

$$\begin{aligned} &[\tilde{r}_{xj}][\tilde{r}_{xj}]\mathbf{s}_{C0}s_{Dx0}^2 + [\tilde{r}_{yj}][\tilde{r}_{yj}]\mathbf{s}_{C0}s_{Dy0}^2 + [\tilde{r}_{zj}][\tilde{r}_{zj}]\mathbf{s}_{C0}s_{Dz0}^2 \\ &\quad + ([\tilde{r}_{yj}][\tilde{r}_{zj}] + ([\tilde{r}_{yj}][\tilde{r}_{zj}])^T)\mathbf{s}_{C0}s_{Dy0}s_{Dz0} \\ &\quad + ([\tilde{r}_{xj}][\tilde{r}_{zj}] + ([\tilde{r}_{xj}][\tilde{r}_{zj}])^T)\mathbf{s}_{C0}s_{Dx0}s_{Dz0} \\ &\quad + ([\tilde{r}_{xj}][\tilde{r}_{yj}] + ([\tilde{r}_{xj}][\tilde{r}_{yj}])^T)\mathbf{s}_{C0}s_{Dx0}s_{Dy0} \end{aligned} \tag{32}$$

Substituting this expression back into Eq. (27) and distributing the summation yields

$$\frac{\partial \mathcal{L}}{\partial \mathbf{s}_{C0}} = [M_{xx}]\mathbf{s}_{C0}s_{Dx0}^2 + [M_{yy}]\mathbf{s}_{C0}s_{Dy0}^2 + [M_{zz}]\mathbf{s}_{C0}s_{Dz0}^2 + [M_{yz}]\mathbf{s}_{C0}s_{Dy0}s_{Dz0} + [M_{xz}]\mathbf{s}_{C0}s_{Dx0}s_{Dz0} + [M_{xy}]\mathbf{s}_{C0}s_{Dx0}s_{Dy0} - [\Sigma\mathcal{R}]^T\mathbf{s}_{D0}R_{CD} + N\mathbf{s}_{C0} + 2\lambda_1\mathbf{s}_{C0} \tag{33}$$

where

$$[M_{xx}] = \sum [\tilde{r}_{xj}][\tilde{r}_{xj}], \quad [M_{yz}] = \sum([\tilde{r}_{yj}][\tilde{r}_{zj}] + ([\tilde{r}_{yj}][\tilde{r}_{zj}])^T),$$
$$[M_{yy}] = \sum [\tilde{r}_{yj}][\tilde{r}_{yj}], \quad [M_{xz}] = \sum([\tilde{r}_{xj}][\tilde{r}_{zj}] + ([\tilde{r}_{xj}][\tilde{r}_{zj}])^T),$$
$$[M_{zz}] = \sum [\tilde{r}_{zj}][\tilde{r}_{zj}], \quad [M_{xy}] = \sum([\tilde{r}_{xj}][\tilde{r}_{yj}] + ([\tilde{r}_{xj}][\tilde{r}_{yj}])^T),$$
$$[\Sigma\mathcal{R}]^T = \sum [\mathcal{R}_j]^T \tag{34}$$

Note that all $[M]$ matrices can be evaluated as static numerical coefficients during problem formulation with no need to evaluate them during the solution process. If desired, the summations of Eq. (34) can be converted to integrals (for an infinite number of discretization steps) at next to no computational cost. Note that $[M]$ matrices are symmetric. The symmetry of Eq. (33) may be appreciated by writing it as

$$\frac{\partial \mathcal{L}}{\partial \mathbf{s}_{C0}} = \left(\mathbf{s}_{D0}^T \sum \begin{bmatrix} [\tilde{r}_{xj}][\tilde{r}_{xj}] & [\tilde{r}_{xj}][\tilde{r}_{yj}] & [\tilde{r}_{xj}][\tilde{r}_{zj}] \\ ([\tilde{r}_{xj}][\tilde{r}_{yj}])^T & [\tilde{r}_{yj}][\tilde{r}_{yj}] & [\tilde{r}_{yj}][\tilde{r}_{zj}] \\ ([\tilde{r}_{xj}][\tilde{r}_{zj}])^T & ([\tilde{r}_{yj}][\tilde{r}_{zj}])^T & [\tilde{r}_{zj}][\tilde{r}_{zj}] \end{bmatrix}\mathbf{s}_{D0}\right)\mathbf{s}_{C0} - [\Sigma\mathcal{R}]^T\mathbf{s}_{D0}R_{CD} + N\mathbf{s}_{C0} + 2\lambda_1\mathbf{s}_{C0} \tag{35}$$

where the first term is written using unconventional notation meant to be intuitive. This term can be interpreted as a summed matrix of matrices where each entry is pre- and post-multiplied by $\mathbf{s}_{D0}$ to form a usual 3×3 matrix which is subsequently multiplied by $\mathbf{s}_{C0}$.

Equations (27)–(35) were dedicated to rearranging Eq. (23) to collect j indexed terms into coefficients. The process of rearranging Eq. (24) is quite similar. We write the result as follows:

$$\frac{\partial \mathcal{L}}{\partial \mathbf{s}_{D0}} = [N_{xx}]\mathbf{s}_{D0}s_{Cx0}^2 + [N_{yy}]\mathbf{s}_{D0}s_{Cy0}^2 + [N_{zz}]\mathbf{s}_{D0}s_{Cz0}^2 + [N_{yz}]\mathbf{s}_{D0}s_{Cy0}s_{Cz0} + [N_{xz}]\mathbf{s}_{D0}s_{Cx0}s_{Cz0} + [N_{xy}]\mathbf{s}_{D0}s_{Cx0}s_{Cy0} - [\Sigma\mathcal{R}]\mathbf{s}_{C0}R_{CD} + N\mathbf{s}_{D0} + 2\lambda_2\mathbf{s}_{D0} \tag{36}$$

where

$$[N_{xx}] = \sum [\tilde{c}_{xj}][\tilde{c}_{xj}], \quad [N_{yz}] = \sum([\tilde{c}_{yj}][\tilde{c}_{zj}] + ([\tilde{c}_{yj}][\tilde{c}_{zj}])^T),$$
$$[N_{yy}] = \sum [\tilde{c}_{yj}][\tilde{c}_{yj}], \quad [N_{xz}] = \sum([\tilde{c}_{xj}][\tilde{c}_{zj}] + ([\tilde{c}_{xj}][\tilde{c}_{zj}])^T),$$
$$[N_{zz}] = \sum [\tilde{c}_{zj}][\tilde{c}_{zj}], \quad [N_{xy}] = \sum([\tilde{c}_{xj}][\tilde{c}_{yj}] + ([\tilde{c}_{xj}][\tilde{c}_{yj}])^T),$$
$$[\Sigma\mathcal{R}] = \sum [\mathcal{R}_j] \tag{37}$$

The $[\tilde{c}_{xj}]$, $[\tilde{c}_{yj}]$, $[\tilde{c}_{zj}]$ matrices are skew symmetrics formed from the columns of $[\mathcal{R}_j]$ as outlined in Eq. (22). Just as before, all $[N]$ matrices are symmetric and may be evaluated before the actual solution process. The symmetry of Eq. (36) may be appreciated by writing it as

$$\frac{\partial \mathcal{L}}{\partial \mathbf{s}_{D0}} = \left(\mathbf{s}_{C0}^T \sum \begin{bmatrix} [\tilde{c}_{xj}][\tilde{c}_{xj}] & [\tilde{c}_{xj}][\tilde{c}_{yj}] & [\tilde{c}_{xj}][\tilde{c}_{zj}] \\ ([\tilde{c}_{xj}][\tilde{c}_{yj}])^T & [\tilde{c}_{yj}][\tilde{c}_{yj}] & [\tilde{c}_{yj}][\tilde{c}_{zj}] \\ ([\tilde{c}_{xj}][\tilde{c}_{zj}])^T & ([\tilde{c}_{yj}][\tilde{c}_{zj}])^T & [\tilde{c}_{zj}][\tilde{c}_{zj}] \end{bmatrix}\mathbf{s}_{C0}\right)\mathbf{s}_{D0} - [\Sigma\mathcal{R}]\mathbf{s}_{C0}R_{CD} + N\mathbf{s}_{D0} + 2\lambda_2\mathbf{s}_{D0} \tag{38}$$

where the same unconventional notation of Eq. (35) is reused. Expansion of Eq. (25) is much simpler

$$\frac{\partial \mathcal{L}}{\partial R_{CD}} = -[\Sigma\mathcal{R}]\mathbf{s}_{C0}\cdot\mathbf{s}_{D0} + NR_{CD} \tag{39}$$

and Eq. (26) requires no expansion.

Equations (26), (33), (36), and (39) reform the system of nine polynomials in nine variables originally formed in Eqs. (23)–(26). A three-homogeneous grouping partitioned by the vector components of $\mathbf{s}_{C0}$, $\mathbf{s}_{D0}$, and the group $\{R_{DC}, \lambda_1, \lambda_2\}$ indicates a Bézout degree of 3564. This polynomial system contains 82 parameters: the six components of each symmetric $[M]$ matrix (34), the six components of each symmetric $[N]$ matrix (37), the nine components of $[\Sigma\mathcal{R}]$, and the number of discretization points N. This is not the smallest parameterization but was found to be sufficiently minimal. Analysis by Bertini found 244 finite, isolated solutions. It can be found that solutions occurred in sets of four characterized by swapped signs between vector components of $\mathbf{s}_{C0}$ and $\mathbf{s}_{D0}$. Namely, for any solution containing $\{\mathbf{s}_{C0}, \mathbf{s}_{D0}\}$ there also existed solutions with $\{\mathbf{s}_{C0}, -\mathbf{s}_{D0}\}$, $\{-\mathbf{s}_{C0}, \mathbf{s}_{D0}\}$, and $\{-\mathbf{s}_{C0}, -\mathbf{s}_{D0}\}$. This stems from the quadratic sphere constraints of Eq. (26). All four solutions indicate the same four-bar, so only one copy from each set is kept, effectively reducing the solution count to 61. Proceeding solutions computed by parameter homotopy continuation then only need to track 61 homotopy paths.

One of the 61 solutions always results in the same degenerate mechanism found in the exact five position synthesis, where $\mathbf{s}_{C0}$ and $\mathbf{s}_{A0}$ are coincident and $\mathbf{s}_{D0}$ and $\mathbf{s}_{B0}$ are coincident. Since this solution meets the objective exactly, it will always be the global minimum of the optimization problem.

This method does not constrain the approximate motion to remain on the same circuit or branch, so defective solutions are possible. However, by computing all critical points, this method provides many alternative solutions when defects are encountered.

6.1 Eigenanalysis of Critical Points. After all of the critical points of Eq. (20) are computed by parameter homotopy continuation, each should be identified as a minimum, saddle, or maximum. It is additionally useful to know the principal directions of curvature of each critical point, see Ref. [15]. Such information is obtained by computing the eigenvalues and eigenvectors of the Hessian. For the case of constrained optimization, the Hessian should be transformed to only consider directions of perturbation that adhere to the constraints.

Consider the minimization of $f(\mathbf{x})$, subject to $\mathbf{h}(\mathbf{x}) = 0$ where $\mathbf{x} \in \mathbb{R}^n$ and $\mathbf{h} \in \mathbb{R}^m$. The gradient $\nabla f(\mathbf{x}) = \dfrac{\partial f}{\partial \mathbf{x}}$ is an $n\times1$ vector, and the Hessian is an $[\mathcal{H}(\mathbf{x})] = \left[\dfrac{\partial^2 f}{\partial \mathbf{x}^2}\right]$ is an $n\times n$ matrix. The second-order Taylor approximation of $f(\mathbf{x})$ about point $\mathbf{a}$ is

$$f(\mathbf{x}) \approx f(\mathbf{a}) + (\mathbf{x}-\mathbf{a})^T\nabla f(\mathbf{a}) + \frac{1}{2}(\mathbf{x}-\mathbf{a})^T[\mathcal{H}(\mathbf{a})](\mathbf{x}-\mathbf{a}) \tag{40}$$

Subtract $f(\mathbf{a})$ from both sides to represent the change in objective. Note that the gradient vanishes at critical points. Then the Hessian term stands alone on the right-hand side to approximate changes in the objective due to perturbations $\Delta\mathbf{x} = \mathbf{x}-\mathbf{a}$. However, we should only study perturbations in directions that adhere to the constraints $\mathbf{h}(\mathbf{x}) = 0$. The derivative $\left[\dfrac{\partial \mathbf{h}}{\partial \mathbf{x}}\right]$ gives an $m\times n$ matrix with row vectors that span the space normal to the constraints. Represent a vector tangent to the constraints as $\mathbf{t}$. Then the equation $\left[\dfrac{\partial \mathbf{h}}{\partial \mathbf{x}}\right]\mathbf{t} = \mathbf{0}$ can simply be interpreted as a listing of orthogonality constraints of $\mathbf{t}$ with the normal space. Computation of the null space of $\left[\dfrac{\partial \mathbf{h}}{\partial \mathbf{x}}\right]$ yields $d = n-m$ basis vectors of

the tangent space. We orthonormalize these basis vectors then place them into the columns of a new $n \times d$ matrix $[T]$. Once $[T]$ is computed, perturbations that adhere to the constraints may be represented as

$$\Delta \mathbf{x} = [T]\Delta \mathbf{y} \tag{41}$$

where the components of $\Delta \mathbf{y}$ parameterize the tangent space. Substituting this into Eq. (40) applies a similarity transformation to the Hessian, $[T]^T[\mathcal{H}(\mathbf{a})][T]$, that reduces it to a $d \times d$ matrix. The product is called the projected Hessian. Its eigenvectors, after being transformed by $[T]$ (41), indicate principal directions of curvature. Its eigenvalues are called principal curvatures, i.e., the second-order information which finds itself leading the Taylor series. Positive eigenvalues indicate directions of ascent, and negative eigenvalues indicate directions of descent. Such criteria are used to identify minima, maxima, and saddle points. Saddle points are further classified as index-k saddles if k of the eigenvalues are negative. It has been shown in another work [15] that characterizing the descent directions of saddles can be useful.

7 Approximate Synthesis for the General Case

The approximate synthesis formulation presented in Sec. 6 presets the ground pivot axes $\mathbf{s}_{A0}$ and $\mathbf{s}_{B0}$. The most general formulation leaves the components of $\mathbf{s}_{B0}$ to vary. Recall from Sec. 3 that, without loss of generality, $\mathbf{s}_{A0} = \{1, 0, 0\}$ and $\mathbf{s}_{B0} = \{s_{Bx0}, s_{By0}, 0\}$. Our goal is to once again minimize Eq. (17) but now subject to an additional circle constraint

$$\min_{\mathbf{s}_{B0}, \mathbf{s}_{C0}, \mathbf{s}_{D0}, R_{CD}} \quad \frac{1}{2}\sum \eta_j^2 \tag{42}$$

$$\text{s.t.} \quad \mathbf{h} := \begin{Bmatrix} \mathbf{s}_{B0} \cdot \mathbf{s}_{B0} - 1 \\ \mathbf{s}_{C0} \cdot \mathbf{s}_{C0} - 1 \\ \mathbf{s}_{D0} \cdot \mathbf{s}_{D0} - 1 \end{Bmatrix} = 0 \tag{43}$$

The Lagrangian takes the same form as Eq. (21) and the stationarity conditions repeat in that Eqs. (23)–(25) must vanish along with the additional partial derivative

$$\begin{aligned} \frac{\partial \mathcal{L}}{\partial \mathbf{s}_{B0}} = \sum \Big(& ([\mathcal{R}(\mathbf{s}_{A0}, \phi_j)]\mathbf{s}_{C0} \cdot [\mathcal{R}(\mathbf{s}_{B0}, \psi_j)]\mathbf{s}_{D0} - R_{CD}) \\ & \cdot (-\sin\psi_j([\mathcal{R}(\mathbf{s}_{A0}, \phi_j)]\mathbf{s}_{C0}) \times \mathbf{s}_{D0} \\ & + (1 - \cos\psi_j)(([\mathcal{R}(\mathbf{s}_{A0}, \phi_j)]\mathbf{s}_{C0}) \times (\mathbf{s}_{D0} \times \mathbf{s}_{B0}) \\ & + \mathbf{s}_{D0} \times (([\mathcal{R}(\mathbf{s}_{A0}, \phi_j)]\mathbf{s}_{C0}) \times \mathbf{s}_{B0}))) \Big) + 2\lambda_3 \mathbf{s}_{B0} \end{aligned} \tag{44}$$

Note that Eq. (44) is a 3×1 vector where the third component is zero since s_{Bz0} is not present. Therefore, we only consider the first two components of Eq. (44). Equations (23)–(25), (43), and (44) form a system of 12 polynomials in 12 variables: two components of $\mathbf{s}_{B0}$, three components of $\mathbf{s}_{C0}$, three components of $\mathbf{s}_{D0}$, R_{CD}, λ_1, λ_2, and λ_3. For neatness, it is more pleasant to order the synthesis equations as (44), (23), (24), (25), and (43), and re-index the Lagrange multipliers to follow the order of Eq. (43). The roots of these equations indicate the critical points of the optimization problem (42).

A four-homogeneous grouping partitioned by the vector components of $\mathbf{s}_{B0}$, $\mathbf{s}_{C0}$, $\mathbf{s}_{D0}$, and the group $\{R_{CD}, \lambda_1, \lambda_2, \lambda_3\}$ indicates a Bézout degree of 621,984. Furthermore, it can be found that solutions appear in sets of eight, which correspond to all sign combinations of $\mathbf{s}_{C0}$ and $\mathbf{s}_{D0}$, plus rotations of 180° about $\mathbf{s}_{A0}$. In other words, a single solution $\{\mathbf{s}_{B0}, \mathbf{s}_{C0}, \mathbf{s}_{D0}, R_{CD}, \lambda\}$, appears in the following set of eight solutions:

$$\begin{aligned} &\{\mathbf{s}_{B0}, \quad \mathbf{s}_{C0}, \quad \mathbf{s}_{D0}, \quad R_{CD}, \ \lambda\} \\ &\{\mathbf{s}_{B0}, \quad \mathbf{s}_{C0}, \ -\mathbf{s}_{D0}, \ -R_{CD}, \ \lambda\} \\ &\{\mathbf{s}_{B0}, \ -\mathbf{s}_{C0}, \quad \mathbf{s}_{D0}, \ -R_{CD}, \ \lambda\} \\ &\{\mathbf{s}_{B0}, \ -\mathbf{s}_{C0}, \ -\mathbf{s}_{D0}, \quad R_{CD}, \ \lambda\} \\ &\{[\mathcal{R}(\mathbf{s}_{A0}, \pi)]\mathbf{s}_{B0}, \quad [\mathcal{R}(\mathbf{s}_{A0}, \pi)]\mathbf{s}_{C0}, \quad [\mathcal{R}(\mathbf{s}_{A0}, \pi)]\mathbf{s}_{D0}, \quad R_{CD}, \ \lambda\} \\ &\{[\mathcal{R}(\mathbf{s}_{A0}, \pi)]\mathbf{s}_{B0}, \quad [\mathcal{R}(\mathbf{s}_{A0}, \pi)]\mathbf{s}_{C0}, \ -[\mathcal{R}(\mathbf{s}_{A0}, \pi)]\mathbf{s}_{D0}, \ -R_{CD}, \ \lambda\} \\ &\{[\mathcal{R}(\mathbf{s}_{A0}, \pi)]\mathbf{s}_{B0}, \ -[\mathcal{R}(\mathbf{s}_{A0}, \pi)]\mathbf{s}_{C0}, \quad [\mathcal{R}(\mathbf{s}_{A0}, \pi)]\mathbf{s}_{D0}, \ -R_{CD}, \ \lambda\} \\ &\{[\mathcal{R}(\mathbf{s}_{A0}, \pi)]\mathbf{s}_{B0}, \ -[\mathcal{R}(\mathbf{s}_{A0}, \pi)]\mathbf{s}_{C0}, \ -[\mathcal{R}(\mathbf{s}_{A0}, \pi)]\mathbf{s}_{D0}, \quad R_{CD}, \ \lambda\} \end{aligned} \tag{45}$$

To solve this system, we applied the method of random monodromy loops [17]. By forming duplicate criteria from Eq. (45), the algorithm was configured to collect sets of solutions at a time, rather than piecemeal. Through random monodromy loops, 268 sets of eight finite, isolated roots were computed in about 5 min on a single thread using a personal computer. To compare the efficiency of our algorithm, we also setup a multihomogeneous homotopy, which took about 20 h on a cluster of 192 cores to produce a similar solution.

8 Design of a Mechanism to Time Wing Deployment

We applied our theoretical work to the design of a mechanism that coordinates unfolding angles for a deployment. The problem statement is visually summarized in Figs. 3 and 4. Each wing rotates around a spatially angled pivot from a compact stowed configuration to a flight-ready deployed configuration. The two spatial wing pivots intersect at a common point with a relative interior angle of 20°. This sets the pre-specification of axes $\mathbf{s}_{A0}$ and $\mathbf{s}_{B0}$. We applied the synthesis solution for approximate function generation by a spherical four-bar with both ground pivots specified.

To improve the structural capabilities of the wings after deployment, the wings possess tabs that cross over each other and span the width of the fuselage. An uncontrolled deployment of this design could result in a collision between the overlapping tabs of the two wings, preventing the wings from reaching their final configuration. Likewise, a 1:1 counter-rotation by means of bevel gears would also result in collision. However, a spherical four-bar is capable of

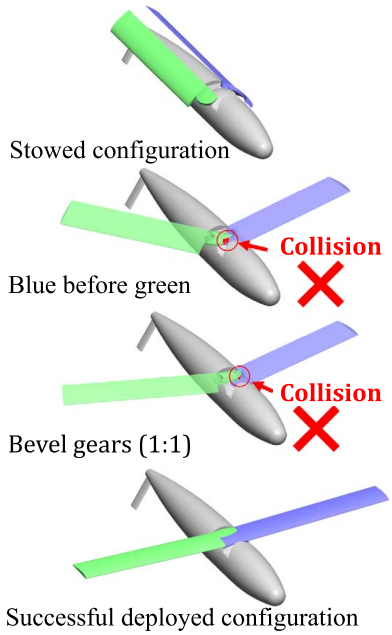

Fig. 3 A spherical four-bar to coordinate the timing of wing deployment

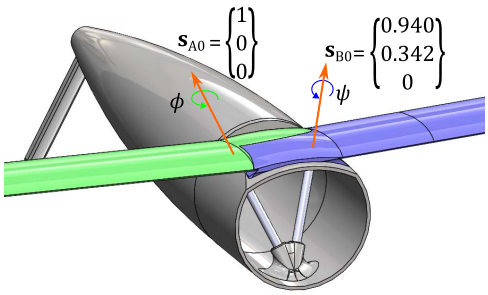

Fig. 4 The aircraft wings rotated around two intersecting spatially angled axis

producing a nonlinear coordination between wing angles ϕ and ψ to allow proper nesting between the wing tabs.

8.1 Function Generation Setup. The setup described in Sec. 3 is applied to this problem, see Fig. 4. To show the pivots, the nose of the UAV has been removed. The pivot axes $\mathbf{s}_{A0}$ and $\mathbf{s}_{B0}$ are in the direction of the joints connecting the wings to the fuselage. The angle pairs must move from the stowed configuration, $(0°, 0°)$, to the fully deployed configuration, $(99.2°, -99.2°)$. Between these configurations, it was required that the two joints counter-rotate in a nonlinear manner to avoid collision. Specifically, the right wing rotates more quickly at the beginning of the deployment to get clear of the left wing. In total, ten angle pairs, (ϕ_j, ψ_j), $j = 0, \ldots, 9$, were chosen, which are listed in Table 1.

8.2 Analysis of Candidate Designs. The approximate synthesis problem was solved using the formulation in Sec. 6. Using parameter homotopy continuation, all 61 critical points were found repeatedly in less than 5 s using a personal computer. Eliminating imaginary solutions and the single known degenerate solution ($\mathbf{s}_{C0} = \mathbf{s}_{A0}$ and $\mathbf{s}_{D0} = \mathbf{s}_{B0}$) resulted in 12 physical solutions. An eigenanalysis of the physical solutions identified three minima and nine saddles. For this application, both ground pivots will be actuated by a cable wrapped around a capstan, so branches in the solutions were not considered an issue. Figure 5 shows the functions produced by each solution, along with each solution's saddle index.

Solution 2 was selected because it is a minimum, it approximates the angle pairs most closely, and it does not pass through any singular configurations. This same function can be produced by four different constructions of the mechanism, which are found by toggling the positive and negative directions of $\mathbf{s}_{C0}$ and $\mathbf{s}_{D0}$. Four different constructions of Solution 2 are shown in Fig. 6. The $(-\mathbf{s}_{C0}, -\mathbf{s}_{D0})$ construction in Fig. 6 fits particularly well within the fuselage of the UAV, so it was selected for implementation.

Table 1 Angle pairs for approximate synthesis

j	ϕ_j	ψ_j
0	0°	0°
1	14.8969°	−4.0107°
2	30.9397°	−10.3132°
3	45.2637°	−16.6158°
4	59.0147°	−25.2101°
5	69.9009°	−34.9504°
6	79.6411°	−46.9825°
7	85.9437°	−63.0254°
8	91.6732°	−81.9330°
9	99.2°	−99.2°

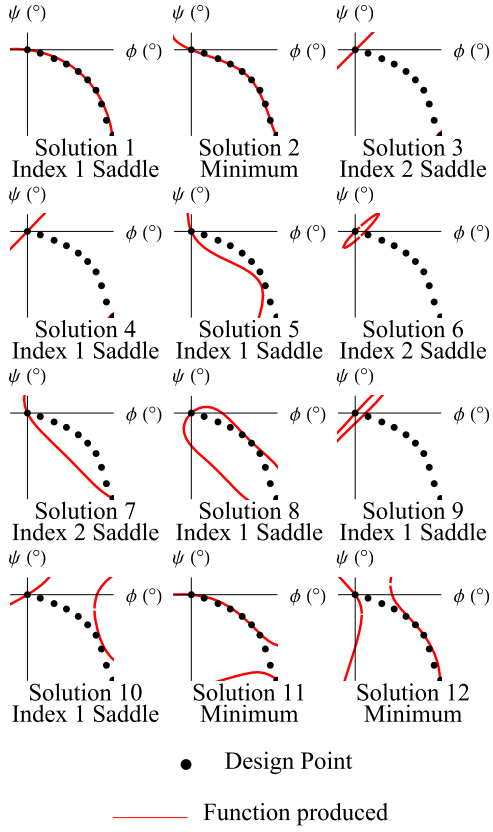

Fig. 5 The coordination of angles exhibited by each of the critical points

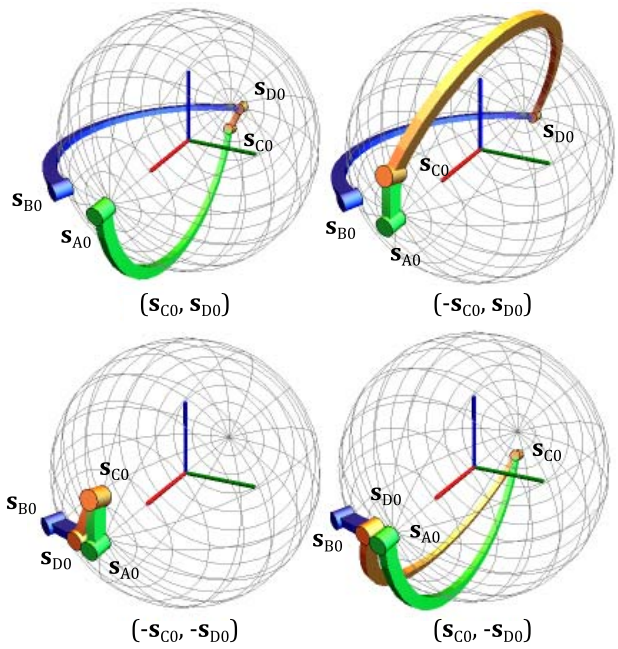

Fig. 6 Each solution corresponds to four different constructions of Solution 2 from Fig. 5

8.3 Implementation of Design. The function generator design was incorporated into a small aircraft fuselage and fabricated using additive manufacturing. The computer-aided design (CAD) model and physical prototype are shown in Fig. 7. Each wing will be actuated by a cable wrapped around a capstan at the joint, and the function generator will facilitate timing coordination between the two wings.

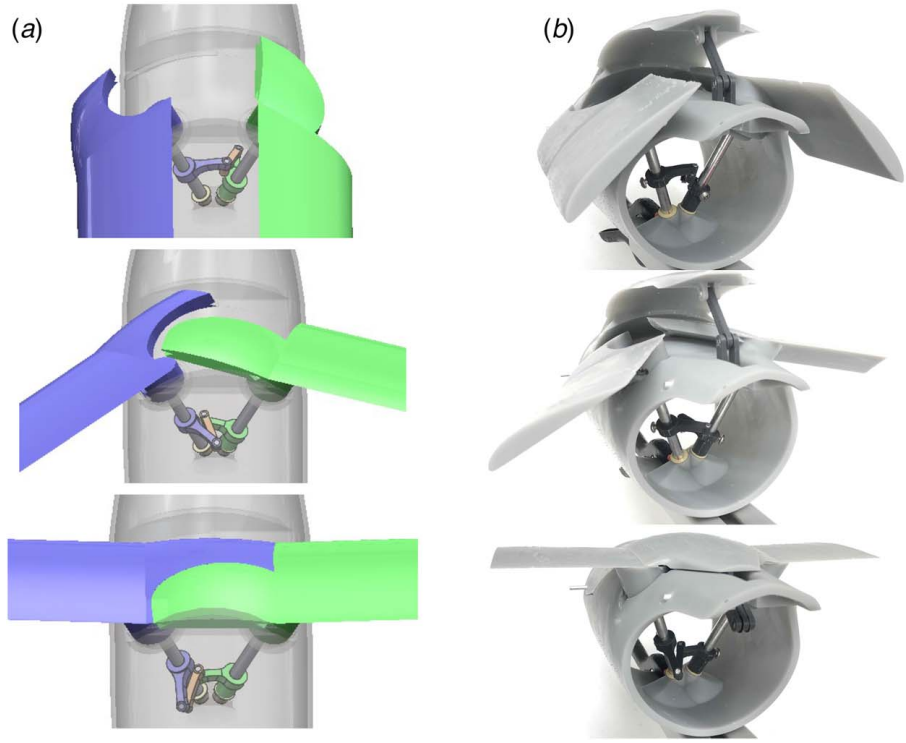

Fig. 7 Prototype of the deployment timing mechanism: (*a*) CAD model and (*b*) physical prototype

9 Analysis of Function Specification

To observe the effects of function specification on our optimization algorithm, the desired function for the deployment mechanism in Sec. 8 was varied. The manually-specified angle pairs in Table 1 form a hyperbola-like curve that allows one of the wings to rotate more quickly than the other at the beginning of the mechanism motion. To generalize this, now we aim to obtain a family of hyperbolas in ϕ–ψ space, parameterized by a

$$\psi = f(\phi, a) := \frac{a}{\phi - b} + c \tag{46}$$

where

$$b = \frac{1}{2}(\phi_0 + \phi_f + d)$$

$$c = \psi_0 + \frac{2a}{-\phi_0 + \phi_f + d}$$

$$d = \sqrt{(\phi_0 - \phi_f)\left(\phi_0 - \phi_f - \frac{4a}{\psi_0 - \psi_f}\right)}$$

This is the family of hyperbolas that pass through points (ϕ_0, ψ_0) and (ϕ_f, ψ_f) with varying curvatures parameterized by a. In the exercise below, we set $(\phi_0, \psi_0) = (0°, 0°)$ and $(\phi_f, \psi_f) = (99.2°, -99.2°)$, similar to the task illustrated above. Twenty curves were specified by changing values of a, from *smooth* ($a = 15$) to *sharp* ($a = 0.025$), see Fig. 8. For each value of a, 100 discretization points, spaced evenly by arc length, were used as angle pairs. The synthesis method in Sec. 6 was performed for each value of a. Between 12 and 14 real, non-degenerate critical points were found for each a, of which exactly three were minima for each case. For each critical point, the objective value was computed from the sum of squares in Eq. (17). The smallest objective value for each a is plotted in Fig. 9. All of these objective values were 10^{-7} or lower, indicating that the hyperbolic curve in Eq. (46) with any a can be nearly perfectly approximated by a spherical four-bar. Plots of the

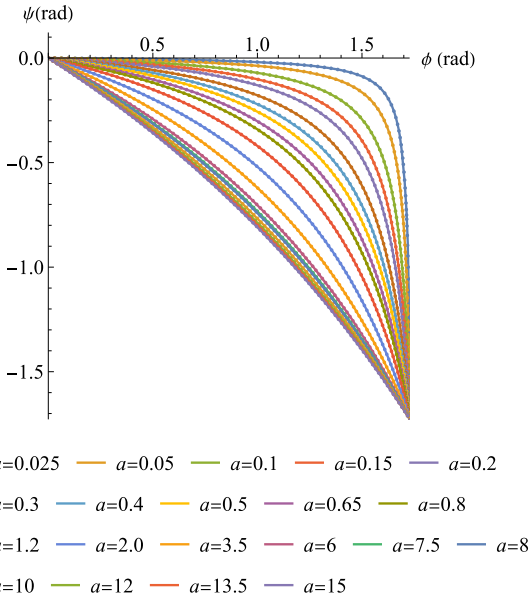

Fig. 8 Curves and discretization points for varied values of *a*

curve produced by the mechanism for each a were found to be visually indistinguishable from Fig. 8. Visualizations of the optimal mechanism produced by four values of a are shown in Fig. 10.

The critical points in Fig. 9 form a curve of solutions in $\mathbb{R}^7$ as a is varied. This suggests that the mechanism dimensions can be directly parameterized by a. The angles between $\mathbf{s}_{A0}$ and $\mathbf{s}_{B0}$, $\mathbf{s}_{A0}$ and $\mathbf{s}_{C0}$; $\mathbf{s}_{B0}$ and $\mathbf{s}_{D0}$; and $\mathbf{s}_{C0}$ and $\mathbf{s}_{D0}$, are given by

$$\begin{aligned} \delta_{AB} &= \arccos(\mathbf{s}_{A0} \cdot \mathbf{s}_{B0}) \\ \delta_{AC} &= \arccos(\mathbf{s}_{A0} \cdot \mathbf{s}_{C0}) \\ \delta_{BD} &= \arccos(\mathbf{s}_{B0} \cdot \mathbf{s}_{D0}) \\ \delta_{CD} &= \arccos(\mathbf{s}_{C0} \cdot \mathbf{s}_{D0}) \end{aligned} \tag{47}$$

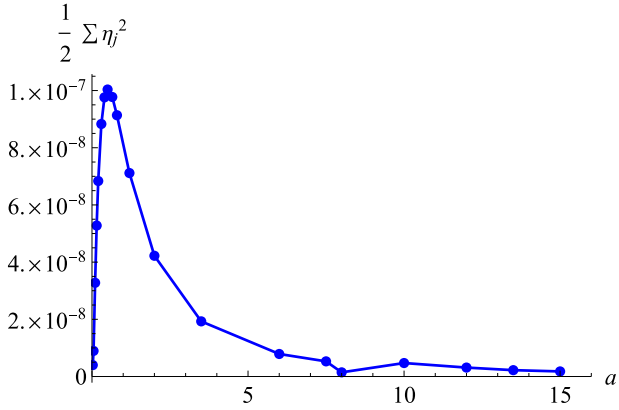

Fig. 9 Smallest objective value for each *a*

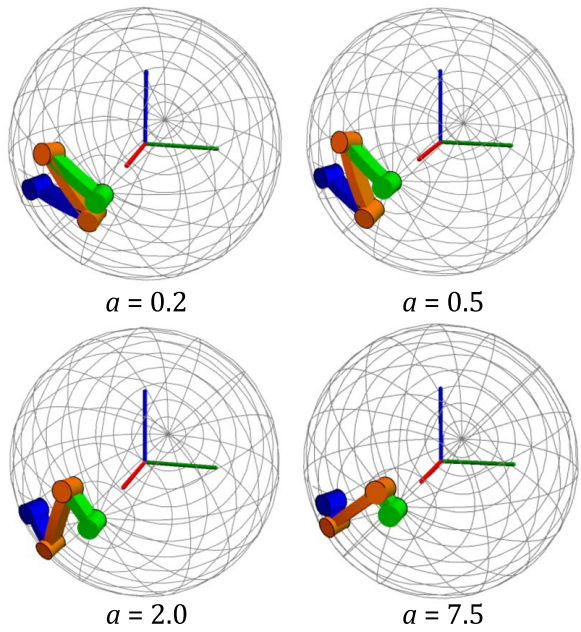

Fig. 10 Mechanism visualizations for $a = 0.2, 0.5, 2.0, 7.5$

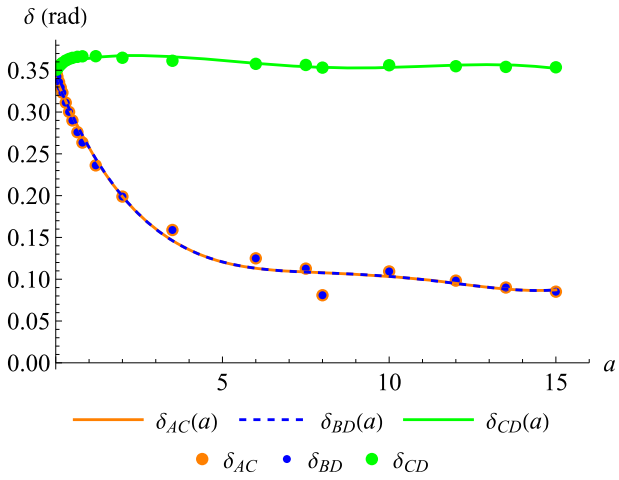

Fig. 11 Mechanism dimensions plotted as a function of *a* and fitted to fourth-order polynomials

where $\delta_{AB} = 20^\circ$ is the specified interior angle between the ground pivots. The optimal values of δ_{AC}, δ_{BD}, and δ_{CD} as a function of a were plotted in Fig. 11, and approximate curves $\delta_{AC}(a)$, $\delta_{BD}(a)$, and $\delta_{CD}(a)$ were constructed using a fourth-order polynomial fit.

Figure 11 shows that for each a, $\delta_{AC} = \delta_{BD}$, meaning the optimal input and output links always have the same dimension. The fitted curves for $\delta_{AC}(a)$, $\delta_{BD}(a)$, and $\delta_{CD}(a)$ are given in Eq. (48)

$$\begin{aligned}\delta_{AC}(a) &= 0.000260557x^4 - 0.00104994x^3 + 0.0152373x^2 \\ &\quad - 0.0971407x + 0.240457 \\ \delta_{BD}(a) &= \delta_{AC}(a), \\ \delta_{CD}(a) &= -(9.9 * 10^{-6})x^4 + 0.000326275x^3 - 0.00341895x^2 \\ &\quad + 0.011249x + 0.356166 \end{aligned} \tag{48}$$

10 Conclusion

Our approach to optimization is not based on iterative local searching. Instead, we form Lagrangian stationarity conditions and compute their complete set of zeros using polynomial homotopy continuation. As a result, we obtain all critical points globally throughout the design space, including all local minima and the global minimum. In this sense, we term our solutions complete. Our approach is applied to the approximate synthesis of spherical four-bar function generation. For the case where both ground pivot directions are specified, the method in this paper can be used to quickly find all 61 sets of critical points of the optimization problem and locate useful designs. For the general case with no prespecification, there are 268 sets of critical points which can quickly be computed. This synthesis procedure was demonstrated in the design of a function generator used to coordinate the deployment timing. For this design, 12 sets of critical points were found, with each corresponding to four constructions of each mechanism. The functionality of the selected mechanism was demonstrated with a physical prototype. Additional analysis was done to observe the effects of changing the specified angle pairs. A parameterized hyperbolic curve was used to specify functions with varying curvatures. The synthesis procedure was applied to each curve, which resulted in a family of mechanisms with near-perfect fit.

Acknowledgment

This work is enabled by financial support from the Air Force Research Lab. We additionally thank Dr. Paul Fleitz from the Air Force Research Lab for many thoughtful discussions about folding wings. This paper has been cleared for public release, Case Number: AFRL-2023-5563. This paper was also supported by the National Science Foundation Grant No. CMMI-2144732.

Conflict of Interest

There are no conflicts of interest.

Data Availability Statement

The datasets generated and supporting the findings of this article are obtainable from the corresponding author upon reasonable request.

Disclosure Statement

Distribution Statement A: Approved for Public Release; Distribution is unlimited. PA# AFRL-2023-5563.

References

[1] Freudenstein, F., 2022, "An Analytical Approach to the Design of Four-Link Mechanisms," Trans. Am. Soc. Mech. Eng., **76**(3), pp. 483–489.

[2] Roth, B., 1967, "Finite-Position Theory Applied to Mechanism Synthesis," ASME J. Appl. Mech., **34**(3), pp. 599–605.

[3] Hartenberg, R. S., and Denavit, J., 1964, *Kinematic Synthesis of Linkages*, McGraw-Hill, New York.

[4] Zimmerman, J. R., 1967, "Four-Precision-Point Synthesis of the Spherical Four-Bar Function Generator," J. Mech., **2**(2), pp. 133–139.

[5] Lakshminarayana, K., 1972, "On the Synthesis of the Spherical Four-bar," Mech. Mach. Theory, **7**(1), pp. 63–69.

[6] Watanabe, K., 1970, "Approximate Synthesis of Spherical Four-Bar Mechanisms," Bull. JSME, **13**(58), pp. 607–615.

[7] Alizade, R. I., and Kilit, Ö., 2005, "Analytical Synthesis of Function Generating Spherical Four-Bar Mechanism for the Five Precision Points," Mech. Mach. Theory, **40**(7), pp. 863–878.

[8] Cervantes-Sánchez, J. J., Gracia, L., Rico-Martínez, J. M., Medellín-Castillo, H. I., and González-Galván, E. J., 2009, "A Novel and Efficient Kinematic Synthesis Approach of the Spherical 4R Function Generator for Five and Six Precision Points," Mech. Mach. Theory, **44**(11), pp. 2020–2037.

[9] Jiawei, W., Xiyuan, C., Shiqi, W., Xiang, L., Ying, Z., and Duanling, L., 2019, "The Algebraic Solution to the Spherical 4R Function Generator for Six Precision Points," 2019 IEEE 9th Annual International Conference on CYBER Technology in Automation, Control, and Intelligent Systems (CYBER), Suzhou, China, July 29–Aug. 2, pp. 42–47.

[10] Rao, S. S., and Ambekar, A. G., 1974, "Optimum Design of Spherical 4-R Function Generating Mechanisms," Mech. Mach. Theory, **9**(3), pp. 405–410.

[11] Liu, Z., and Angeles, J., 1992, "Least-Square Optimization of Planar and Spherical Four-Bar Function Generator Under Mobility Constraints," ASME J. Mech. Des., **114**(4), pp. 569–573.

[12] Sancibrián, R., Garcia, P., Fernández, A., and Viadero Rueda, F., 2007, "Optimal Synthesis of Function Generating Spherical and RSSR Mechanisms," 12th IFToMM World Congress, Besançon, France, June 18–21, pp. 18–21.

[13] Alizade, R., and Gezgin, E., 2011, "Synthesis of Function Generating Spherical Four Bar Mechanism for the Six Independent Parameters," Mech. Mach. Theory, **46**(9), pp. 1316–1326.

[14] Farhang, K., and Zargar, Y. S., 1999, "Design of Spherical 4R Mechanisms: Function Generation for the Entire Motion Cycle," ASME J. Mech. Des., **121**(4), pp. 521–528.

[15] Baskar, A., Plecnik, M., and Hauenstein, J. D., 2022, "Computing Saddle Graphs Via Homotopy Continuation for the Approximate Synthesis of Mechanisms," Mech. Mach. Theory, **176**, p. 104932.

[16] Morgan, A. P., and Sommese, A. J., 1989, "Coefficient-Parameter Polynomial Continuation," Appl. Math. Comput., **29**(2), pp. 123–160.

[17] Baskar, A., and Plecnik, M., 2020, "Synthesis of Six-Bar Timed Curve Generators of Stephenson-type Using Random Monodromy Loops," ASME J. Mech. Rob., **13**(1), p. 011005.

[18] Bates, D. J., Hauenstein, J. D., Sommese, A. J., and Wampler, C. W., 2006, Bertini: Software for Numerical Algebraic Geometry.